SCIENTIFIC REPORTS

OPEN

SUBJECT AREAS:
QUANTUM DOTS
NANOPHOTONICS AND PLASMONICS

Received
12 July 2013

Accepted
2 September 2013

Published
16 September 2013

Correspondence and requests for materials should be addressed to D.G. (davy.gerard@utt.fr) or P.M. (patrice.miska@univ-lorraine.fr)

Plasmonic engineering of spontaneous emission from silicon nanocrystals

Julie Goffard[1,2], Davy Gérard[1], Patrice Miska[2], Anne-Laure Baudrion[1], Régis Deturche[1] & Jérôme Plain[1]

[1]Laboratoire de Nanotechnologie et d'Instrumentation Optique (LNIO), Université de Technologie de Troyes, 12 rue Marie Curie, CS 42060, 10004 Troyes cedex, France, [2]Institut Jean Lamour, CNRS/Nancy Université/UPV Metz, Bd des aiguillettes, 54500 Vandoeuvre-les-Nancy, France.

Silicon nanocrystals offer huge advantages compared to other semi-conductor quantum dots as they are made from an abundant, non-toxic material and are compatible with silicon devices. Besides, among a wealth of extraordinary properties ranging from catalysis to nanomedicine, metal nanoparticles are known to increase the radiative emission rate of semiconductor quantum dots. Here, we use gold nanoparticles to accelerate the emission of silicon nanocrystals. The resulting integrated hybrid emitter is 5-fold brighter than bare silicon nanocrystals. We also propose an in-depth analysis highlighting the role of the different physical parameters in the photoluminescence enhancement phenomenon. This result has important implications for the practical use of silicon nanocrystals in optoelectronic devices, for instance for the design of efficient down-shifting devices that could be integrated within future silicon solar cells.

The efficiency of third generation silicon solar cells is limited by their ability to convert the whole solar spectrum into charge carriers. Due to thermalisation of the charge carriers, the external quantum efficiency (EQE) of silicon solar cells drops in the high-energy region of the spectrum. Spectral conversion of one high-energy photon into two (down-conversion) or one (down-shifting) lower energy photons is a route to reduce these energy losses[1]. Among the possible materials for down-shifting, silicon nanocrystals (SiNCs) are an appealing choice. SiNCs are compatible with silicon-based solar cells and exhibit significant room-temperature photoluminescence (PL)[2]. This luminescence stems from the quantum confinement of the photo-generated excitons and can be tuned in the visible and near-infrared ranges by changing the size of the nanocrystal[3]. Various silicon nanocrystals elaboration techniques have been previously demonstrated such as chemical etching[4], ionic implantation[5,6] or ultra-vacuum evaporation[7]. The use of SiNCs as down-shifters in solar cells has already been demonstrated[8]. However, due to the indirect nature of the bandgap in bulk silicon, the radiative emission rate of SiNCs remains relatively low – considerably hindering the use of SiNCs for solar cells applications. This is why new techniques allowing engineering the emission rate of SiNCs are required. In this regard, plasmonics offers an appealing route. Metal nanostructures exhibiting localized surface plasmon (LSP) resonances are known to modify the emission rate of nearby emitters[9], leading to either quenching or enhancement of the fluorescence emission depending on the experimental conditions[10–14]. Plasmonic engineering of the emission rate is routinely performed with organic molecules or quantum dots, but the number of studies devoted to SiNCs is rather restricted. Pioneering work has been performed by Biteen *et al.* with nanoporous gold[15], evidencing a four-fold enhancement of SiNCs' photoluminescence. Further studies have dealt with the coupling between SiNCs and plasmonics nanostructures such as Ag nanodisks[16], metallic gratings[17–19], and Ag nanotriangles[20]. However, in most of these works, information obtained on coupling was limited by the contribution of uncoupled SiNCs, which were not located at a controllable distance of the metallic particles. New structures with control on all the relevant opto-geometrical parameters are required to gain precise information on the process of coupling between SiNCs and LSP resonances.

In this Communication, we design a hybrid emitter that is 5-fold brighter than bare SiNCs. The hybrid structure consists of gold nanodisks (GNDs) located at a controllable distance from a monolayer of SiNCs. The coupling efficiency, and thus the brightness of the hybrid emitter, strongly depends on the GND-emitter distance, conditioning the photoluminescence quenching and enhancement regimes. Moreover, thanks to luminescence saturation measurements and decay time analysis, we are able to gain insight into the SiNCs luminescence kinetics (radiative rate and quantum yield alteration). A 3.6-fold enhancement of the SiNCs' radiative emission rate is demonstrated. The angular distribution of the photoluminescence emission is also analyzed, quantifying the luminescence redirection (antenna effect). This analysis is enabled thanks to an original method for sample

fabrication allowing to tune under control all the relevant opto-geometrical parameters, such as SiNC-GND distance and the LSP spectral position.

Results

Sample design and fabrication. SiNCs are fabricated by ultra-vacuum evaporation of successive SiO_2/SiO/SiO_2 layers and subsequent thermal annealing[21,22]. After annealing, a dense (10^{12} crystals/cm^2) layer of SiNCs is obtained at a controllable distance from the surface. To obtain plasmonic resonances, gold has been chosen because of its stability in time (no oxidation) and for the matching between plasmonic resonance and SiNCs' emission. The GNDs are fabricated using standard electron beam lithography. During this process, it is of crucial importance to ensure that all SiNCs will be coupled to a plasmonic particle. Hence, an aluminum mask first protects the GNDs before performing a physical etching (Reactive Ion Etching) of the sample in order to remove SiNCs located in between the gold nanodisks. The detailed fabrication procedure is presented in the Methods Section. A 3D schematic of the resulting structure is shown in **Fig. 1a**. In this figure, the red dots stand for the SiNCs position, showing that all SiNCs are located under a GND. Scanning Electron Microscopy (SEM) images of GNDs exhibiting diameters from 140 nm to 220 nm are presented in **Fig. 1b**. Giving the SiNC density, the number of SiNCs under each GND is estimated to be about 600 to 1500, depending on GND's diameter. By changing this diameter, the LSP resonance can be tuned. In **Fig. 1c** is reported the evolution of the extinction spectra by varying the GND diameter and one can observe there is a linear dependence between extinction peak position and GND diameter. It is therefore easy to match the maximum of GND extinction with the maximum of SiNC's emission, which is presented in **Fig. 1d**. This spectrum presents two distinct features: an intense peak around 780-nm arising from quantum confinement in the nanocrystals, and a sideband at lower wavelengths (550–600 nm) that is generally attributed to surface defects at the Si/SiO_2 interface[23]. The maximum of emission coincides with the extinction spectrum of GND with 180 nm in diameter, so the best PL enhancement (i.e. the ratio between the photoluminescence with gold and without gold) is expected at this diameter. The distance between SiNCs and GND is another parameter that can be tuned easily by changing the height of the second SiO_2 layer. We have studied the coupling for distances ranging from 4-nm to 20-nm with a 2-nm step.

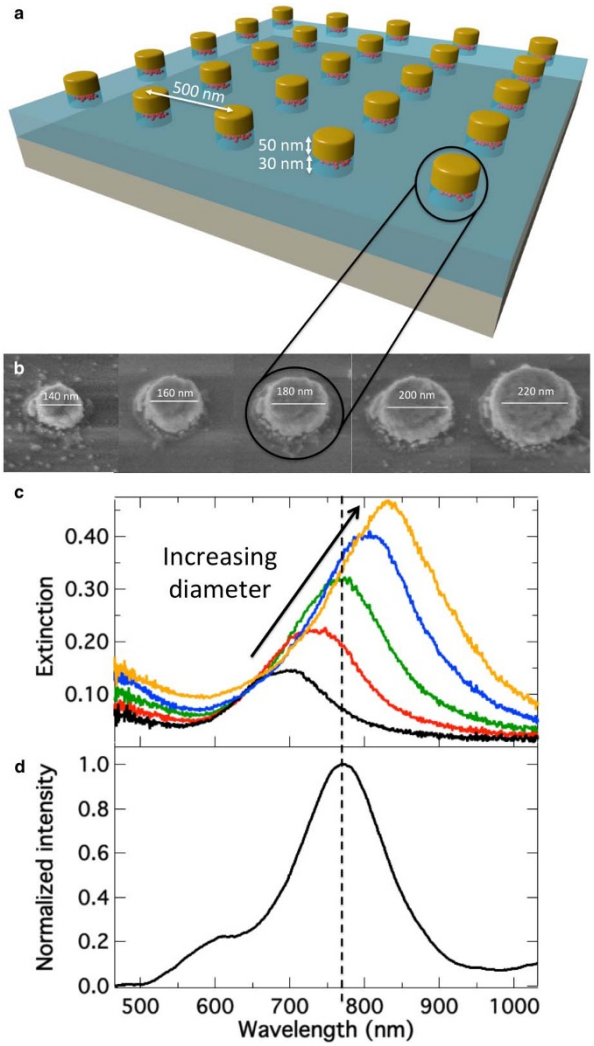

Figure 1 | (a) Schematic of the structure: a monolayer of SiNCs embedded in SiO_2 and at a controllable distance from GND. (b) SEM images of different GND diameters on SiO_2 after etching. (c) Extinction spectra of different GND diameters. (d) Photoluminescence spectrum of SiNCs.

Photoluminescence enhancement and quenching. First, we present the modification of SiNCs' photoluminescence in presence of gold. The analysis is made using the micro-photoluminescence setup described in the Methods Section. **Figures 2a and b** show the SiNCs' photoluminescence for respectively 4-nm and 8-nm spacer thicknesses. The GND's diameter is set to 180-nm, corresponding to a match between plasmon resonance and SiNCs' emission. For a 4-nm spacer thickness, quenching of SiNCs' photoluminescence is evidenced. When the distance is increased to 8 nm, the enhancement regime is observed since the photoluminescence in the presence of GND is almost five times higher than the signal without GND. In order to analyze the distance-dependent behavior of the SiNCs' emission, we have plotted in **Fig. 2c** the PL enhancement, taken at the SiNCs' emission peak, as a function of the SiNC-GND distance. **Figure 2c** evidences a quenching of SiNCs' photoluminescence (PL enhancement below 1.0) for small distances and enhancement at larger distances. An optimum distance of 8-nm is observed where the PL enhancement reaches almost five. This optimum distance stems from a trade-off between the radiative and non-radiative rates enhancement induced by the presence of the gold particle. Such a behavior has been already observed with single molecules[10,11], but to the best of our knowledge it is the first time it is observed with SiNCs. In previous works[15], quenching of luminescence at small distances was not observed because it was hidden by the presence of uncoupled SiNC. In contrast, in our case all SiNCs are coupled to a plasmonic particle unveiling the whole distance-dependent coupling.

Spectral tuning of photoluminescence. Then, we studied the influence of the LSP resonance spectral position. We changed the GND diameter and we compared the PL enhancement with the GND extinction spectra. Results are shown in **Fig. 3a**. It can be noticed that the PL enhancement presents a peak at the same wavelength than the plasmon resonance. Moreover, if the plasmon resonance is shifted, the photoluminescence enhancement peak follows the same shift. It can be also seen that the maximum of enhancement is obtained with a diameter of 180 nm when the plasmon resonance coincides with the maximum of SiNCs' photoluminescence (**Figure 1**). This result suggests dependence between the PL enhancement and the spectral overlap between the plasmon resonances and the SiNCs' photoluminescence. The spectral overlap between plasmon resonance and SiNCs' photoluminescence is determined as the ratio between the overlapping area and the total area below the two spectra. In **Fig. 3b**, the PL enhancement and the spectral overlap are plotted on the same graph as a function of the GND diameter. The PL enhancement is found to follow the same behavior than the spectral overlap.

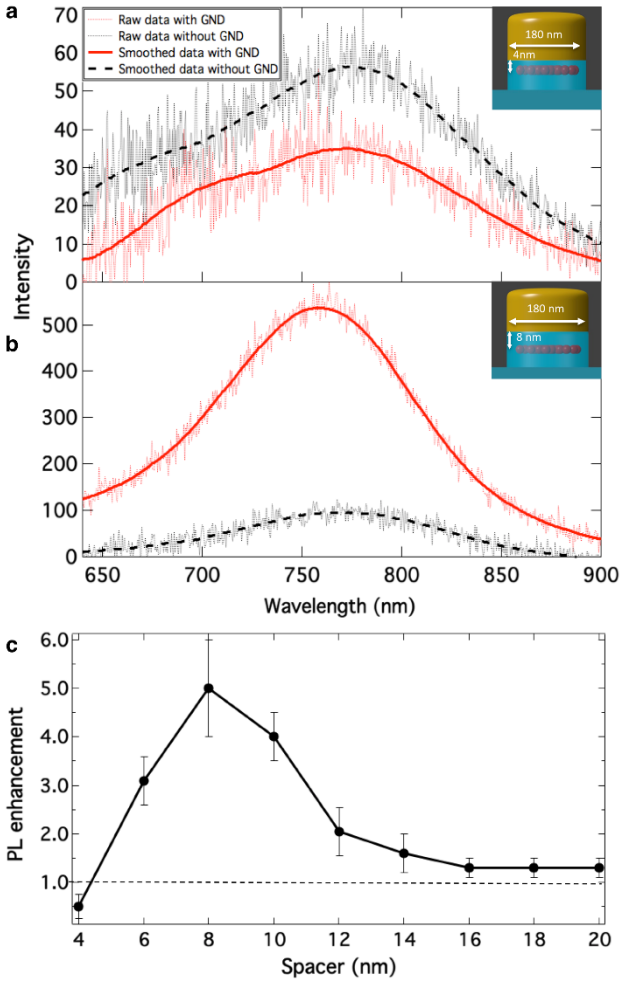

Figure 2 | (a), (b) SiNCs photoluminescence spectra with and without GND for respectively 4 nm and 8 nm in distance between 180 nm-diameter GND and SiNC. (c) Photoluminescence enhancement versus spacer thickness. The dotted line delimits the enhancement and quenching regimes. In each case the excitation power measured at the entrance of the objective is 1 mW.

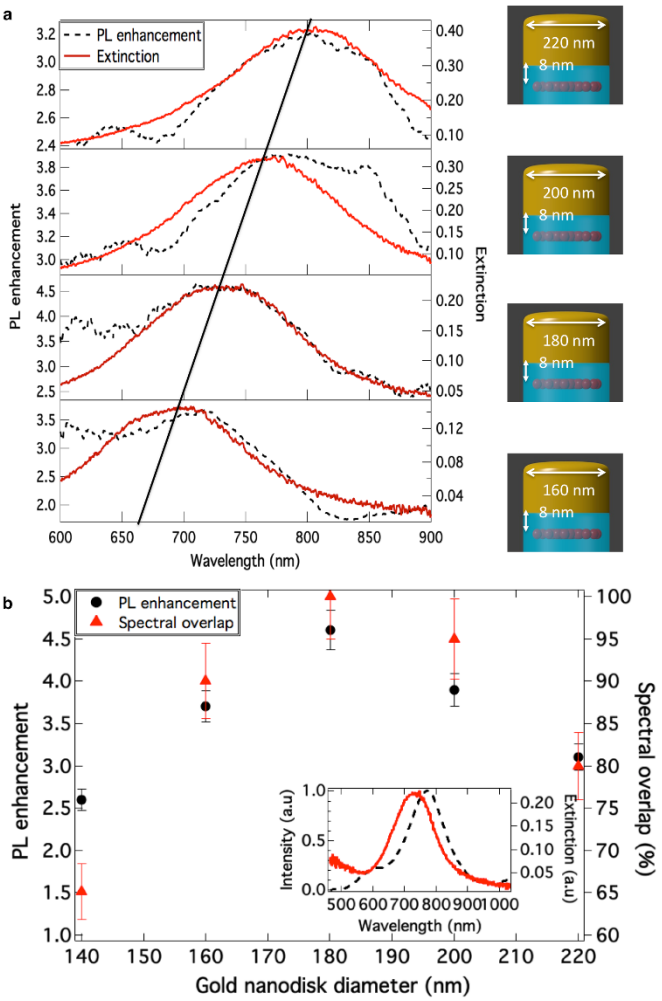

Figure 3 | (a) Comparison between SiNC's photoluminescence enhancement and plasmon resonance position, for four different GND diameters. The black line is a guide for the eye indicating the position of the maximum PL enhancement. (b) Comparison between PL enhancement (black circles) and spectral overlap (red triangles) in function of GND diameter. Inset: example of spectral overlap between SiNCs' photoluminescence (dashed lines) and LSP extinction (continuous line) for a GND diameter of 160 nm.

Redirection of photoluminescence. The presence of the GND can also modify the SiNCs' emission pattern (antenna effect)[24]. To evidence this phenomenon we measured the PL intensity in the back focal plane (Fourier plane or momentum space) of the water objective, this intensity being directly related to the angular distribution of the emitted luminescence. **Figure 4a** shows pictures taken by a camera placed in the back focal plane of the microscope objective, in the absence (left panel) or in the presence (right panel) of a GND. Two circles can be observed. Starting from the inside, the first circle corresponds to the critical angle for SiO_2-air interface (41°) and the second one is the maximum collection angle of the NA = 1.2 immersion objective (53°)[25]. On the left panel of Figure 4a (i.e. without GND) a homogeneous PL intensity distribution can be observed for angles lower than the critical angle, as expected for a single layer of emitters. In contrast, when the GND is added, a strong redirection of the emission toward the objective is observed. In **Fig. 4b**, polar graphs of previous images have been plotted to show the angular dependence of SiNCs' photoluminescence with and without GND. On the left graph, there is no dependence on the angle of SINC's photoluminescence compared to right graph where photoluminescence enhancement is more important for small angles. The GND plays the role of an antenna, directing more luminescence towards the objective and thus contributing to the photoluminescence enhancement. To estimate this contribution, we compared the collection coefficient of the experiment with and without GND. The calculation is presented as **Supplementary Information**, and we estimate of the collection efficiency enhancement to be 1.7. As the total PL enhancement factor reached 5, another phenomenon is needed to explain the enhancement factor.

The same calculation has been performed for all other GND diameters (see **Supplementary Information**, **Fig. S2**). Interestingly, we found the same value of 1.7 for the collection efficiency enhancement. The antenna effect induced by the GND appears to be the same for all studied nanoparticle sizes.

Discussion

The observed enhancement of photoluminescence stems from the modification of the photonic local density of states induced by the presence of GND. According to Fermi's golden rule, the emission rate of a quantum emitter is directly proportional to the local density of states as probed by the emitter. Consequently, the SINCs' radiative emission rate can be increased by the presence of the gold particle, the LSP resonance yielding new plasmonic routes for radiative

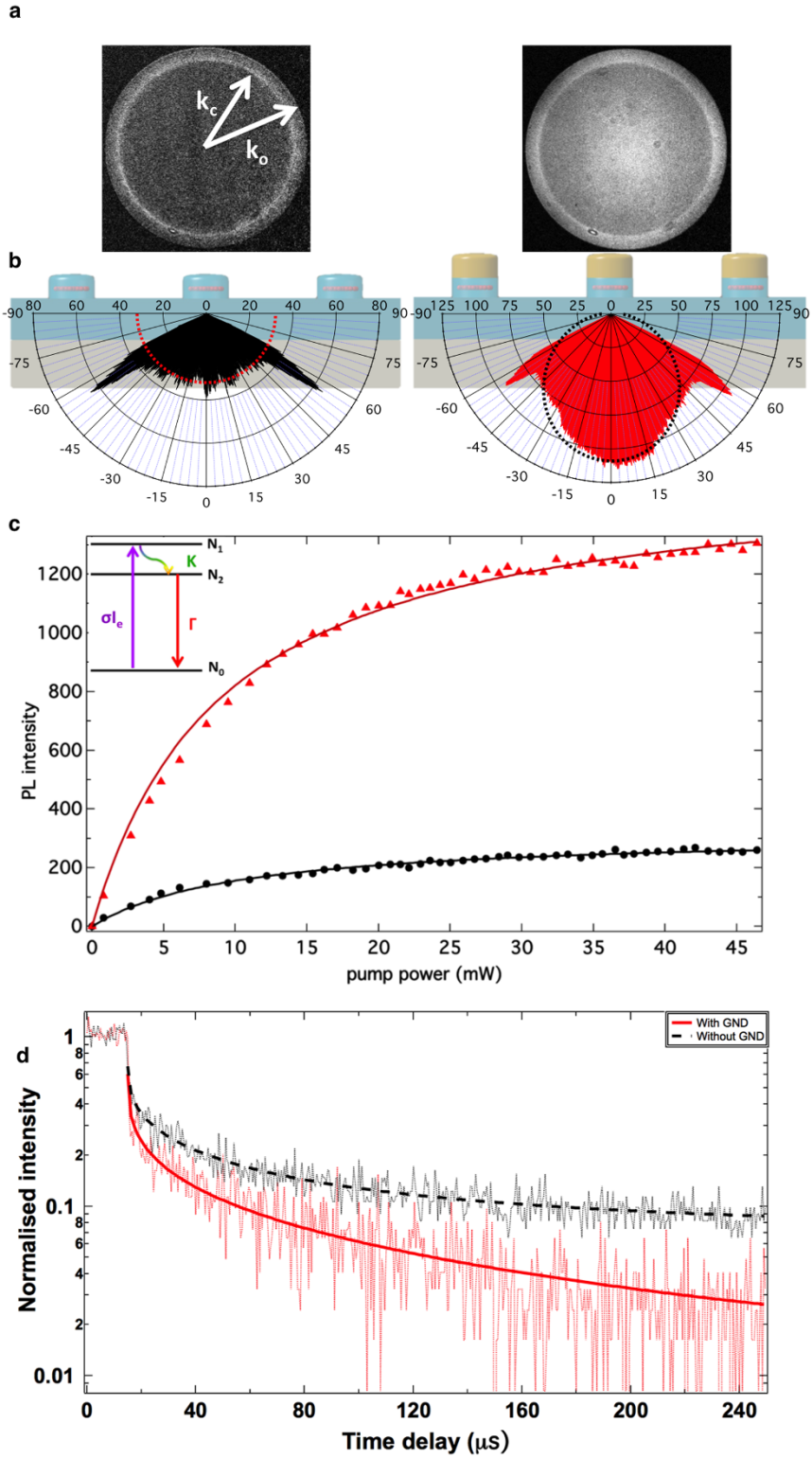

Figure 4 | (a) Photoluminescence distribution in the Fourier plane without gold (left) and with gold (right) for a 180-nm GND located at 8-nm from the SiNCs layer. In the left image k_c is the wave vector corresponding to the critical angle of the air/glass interface and k_o is the maximum wave vector collected by the objective. (b) Polar graph of profiles taken in the Fourier plane, the dotted lines are fits (see Supplementary Information). (c) Photoluminescence versus pump power with GND (red triangles) and without GND (black circles). Continuous lines are numerical fits according to a three-level model (Eq. 6). Fitting parameters are: with a GND (solid red line) A = 162 counts/mW and I_s = 10 mW; without a GND (solid black line) A = 30 counts/mW and I_s = 8.9 mW. Inset: three-level model of the SiNCs. (d) Luminescence decay time measurements with GND (red line) and without GND (black line). Thick lines are numerical fits using a stretched exponential function $I(t) = A.\exp\left(\frac{-t}{\tau}\right)^{\beta}$. Fitting parameters are with a GND (solid red line) A = 0.6, τ = 10.5 μs, β = 0.5; and without a GND (dashed black line) A = 0.6; τ = 15.1 μs; β = 0.5.

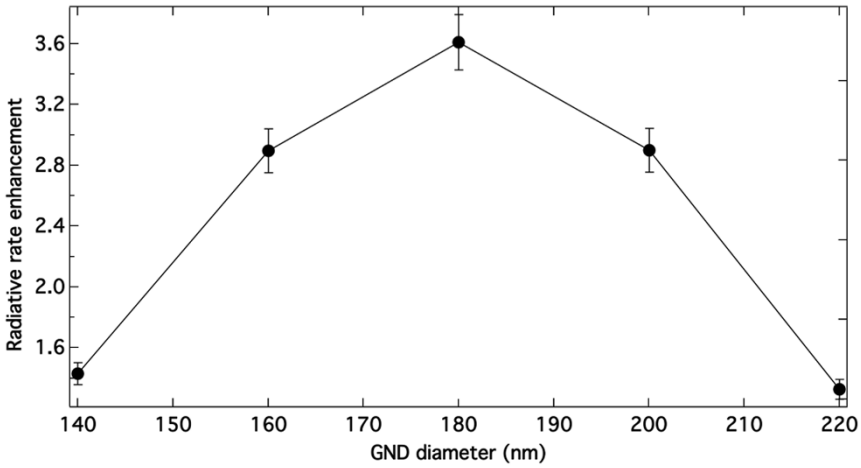

Figure 5 | Radiative rate enhancement as a function of GND diameter.

deexcitation. To demonstrate this assumption, we extracted the different luminescence kinetic rates using the method previously described by Wenger *et al.*[26]. First, we extract SiNCs' luminescence emission rate enhancement η_{Γ_R} (the ratio between SiNCs' emission rate with gold and without gold) from measurements of the PL intensity as a function of the pump power (**Fig. 4c**). If we model the SiNCs as three-level quantum emitters (see **Fig. 4**, inset), the photoluminescence intensity in steady state I_{PL} is given by[26]:

$$I_{PL} = N\kappa \frac{\Gamma_R}{\Gamma} \sigma \frac{I_e}{1+\frac{I_e}{I_s}} \quad (1)$$

Where N is the number of active emitting centers, κ is the collection coefficient of the setup, Γ_R is the radiative emission rate, Γ is the total decay rate (i.e. sum of radiative and non radiative emission rates), and the ratio between Γ_R and Γ is the radiative quantum efficiency Φ, σ is the absorption cross section, I_e is the excitation intensity and I_s the saturation intensity equal to:

$$I_s = \frac{\Gamma}{\sigma} \quad (2)$$

When $I_e \ll I_s$ (weak excitation regime) equation 1 becomes:

$$I_{PL,low} = N\kappa\Phi\sigma I_e \quad (3)$$

Equation 3 shows that in the weak excitation regime, SiNC's photoluminescence intensity is proportional to the excitation rate. When $I_e \gg I_s$ (saturation regime) equation 1 becomes:

$$I_{PL,sat} = N\kappa\Phi\sigma I_s = N\kappa\Gamma_R \quad (4)$$

Equation 5 shows that in the saturation regime P_s becomes constant and is essentially given by the radiative emission rate Γ_R. The radiative emission rate enhancement is defined as:

$$\eta_{\Gamma_R} = \frac{\Gamma_R}{\Gamma_R^0} = \frac{I_{PL,sat}\kappa^0}{I_{PL,sat}^0\kappa}\frac{N^0}{N} \quad (5)$$

Where the superscript '0' stands for SiNCs without GND. Thanks to the etching process during sample fabrication, the number of SiNCs is the same with GND and without GND $N = N^0$. To determine the radiative emission rate enhancement η_{Γ_R}, we have determined the photoluminescence enhancement in the saturation regime $\eta_{I_{PL,sat}} = \frac{I_{PL,sat}}{I_{PL,sat}^0}$ from **Fig. 4c**, and the collection efficiency modification of our experiment $\eta_\kappa = \frac{\kappa}{\kappa^0}$ from **Fig. 4b**, as explained before. To determine $\eta_{I_{PL,sat}}$ the two curves in **Fig. 4c** have been fitted with the function:

$$I_{PL} = A\frac{I_e}{1+\frac{I_e}{I_s}} \quad (6)$$

Thus, from equation 6 we obtain:

$$\eta_{I_{PL,sat}} = \frac{I_{PL,sat}}{I_{PL,sat}^0} = \frac{AI_{sat}}{A^0 I_{sat}^0} = 6.1 \quad (7)$$

Thus the photoluminescence enhancement in saturation regime reached 6 fold for a GND diameter of 180 nm and a SiNC-GND distance of 8 nm. The setup collection efficiency η_κ has been estimated at 1.7 (supporting information). Those two results lead to the determination of η_{Γ_R}. We obtain $\eta_{\Gamma_R} = 3.6$ for the enhancement of the radiative emission rate in presence of GND.

Finally, we estimate the SiNCs' quantum yield modification induced by the presence of the gold particles. Time-resolved photoluminescence measurements have been performed on samples with and without GNDs. Results are presented on **Fig. 4d**. The experimental data have been fitted with a stretched exponential function to extract the decay times. A stretched exponential is used rather than a mono-exponential decay to account for the size distribution of nanocrystals, each size presenting a slightly different decay time[27]. A significant reduction of the decay time is observed in the presence of GNDs, indicating an increase of the total luminescence decay rate. This process gives us an enhancement in total decay rate $\eta_\Gamma = \frac{\Gamma}{\Gamma^0} = 1.58$. From this measurement, the quantum yield enhancement can be deduced as $\eta_\Phi = \frac{\Gamma_R}{\Gamma_R^0}\frac{\Gamma^0}{\Gamma} = 2.25$.

We also studied the influence of GND diameter by performing measurements of the PL intensity vs. pump power for all particle diameters (data not shown). Since the collection efficiency remains the same for all these diameters, it is possible thanks to Eq. 5 to extract the radiative rate enhancement. Results are presented in **Fig. 5**. It appears that the radiative rate enhancement follows the total PL enhancement (**Fig. 3b**), further highlighting the role of surface plasmon in the luminescence enhancement. The closer the plasmon resonance wavelength is from the SiNC emission wavelength, the higher the LDOS and the radiative emission rate are.

In brief, we designed an original hybrid structure allowing plasmonic enhancement of the spontaneous emission from SiNCs. We evidenced a 6-fold enhancement at saturation of the photoluminescence of Si nanocrystals coupled with a 180-nm gold nanodisk, provided that there is an 8-nm spacer between the SiNCs layer and the GND. The distance-dependent luminescence enhancement is shown to be similar in shape to the one observed with single quantum

emitters, even if we deal here with hundreds of silicon emitters. We showed this photoluminescence enhancement had two main origins: (i) a 1.7-fold increase of the collection efficiency due to an antenna effect efficiently redirecting light toward the detector, and (ii) a 3.6-fold increase of the radiative rate (Purcell effect). In this work, only the emission process has been engineered, as the plasmon resonance was tuned to match the SiNCs' emission wavelength. The SiNCs' photoluminescence can be further improved by designing a dual-resonance plasmonic structure, which can enhance simultaneously the excitation and the emission of SiNCs' luminescence. Such a structure could lead to enhancement factors higher than an order of magnitude, enough to obtain efficient emitters for practical applications, such as photovoltaics and Si-based light-emitting devices.

Methods

Sample fabrication. SiNCs are fabricated with evaporation of successive SiO_2/SiO/SiO_2 layers in an ultra-vacuum evaporator[21,28]. The SiO layer is made by thermal evaporation and the two SiO_2 layers are performed with electron beam evaporation. The deposition rate is equal to 0.1 nm.s^{-1} and is controlled by a quartz microbalance system. The thickness of SiO layer and the first SiO_2 layer are constant and equal to respectively 4 nm and 20 nm. The last SiO_2 layer is varied from 4 to 20 nm. The height of this layer determines the distance between SiNC and GND. The sample is then annealed under N_2 gas at a temperature equal to 1050°C during 5 min. This step creates SiNC by dissociation of SiO into Si and SiO_2; the silicon dioxide layers are barrier layers, limiting the size of the resulting nanocrystals. A second annealing treatment under a mixture of N_2 and H_2 (forming gas) is made in order to passive surface defects and improves SiNCs' photoluminescence[29,30].

After SiNC realization, gold nanodisks are fabricated onto the substrate by standard e-beam lithography. First, a layer of polymethylmethacrylate (PMMA) is insolated with an electron beam, in order to pattern arrays of circles. After developing the resist, 3-nm TiO_2 (for improved adhesion), 50-nm gold and 20-nm aluminum layers are deposited onto the structure by electron beam evaporation. After lift off, arrays of cylindrical gold nanodisks with a pitch of 500 nm and diameters varying from 140 nm to 220 nm by step of 20 nm are obtained. The last step of this fabrication is an etching of the sample using reactive ion etching with 17 sccm of SF_6 and 6 sccm of O_2. During this step the aluminum layer protects the gold nanodisks. This step allows us to remove all SiNCs that are not located under a gold nanoparticle. Finally, aluminum is removed with a solution of KOH.

Confocal extinction measurement. Extinction measurements are performed with an Olympus confocal microscope IX71 and a 60 ×, NA = 1.2 water-immersion objective. The sample is illuminated by a halogen lamp and the transmitted signal is collected with the objective. The signal is then sent onto the core of an optical fiber acting as a spatial filter. This defines a confocal detection zone of about 3 μm in diameter. The collected signal is finally sent to a spectrometer (Princeton Instruments ActonSP2300) equipped with a CCD camera (Princeton Instruments Pixis100).

Confocal photoluminescence measurement. The photoluminescence measurement is performed on the same confocal microscope as the extinction measurement. The sample is illuminated from below through the fused silica substrate with a mercury lamp filtered at 400 nm. The resulting luminescence is then collected via the same path (epi-fluorescence) and sent to the spectrometer.

Time-resolved photoluminescence analysis. Time-resolved luminescence is performed using a 405-nm laser diode, electrically modulated using a 1 kHz square signal. This laser illuminates the sample in epi-fluorescence geometry. A photomultiplier tube (PMT) collects the luminescence from the sample. Two filters are placed in front of the PMT, the first is a long pass filter at 500-nm to remove laser reflection and the second filter is a band pass filter centered at 794-nm with a width of 100-nm to collect the SiNC's luminescence. The signal from the PMT is analyzed thanks to a photon counting module (SR400 from National Instruments) and a homemade software. The temporal resolution is mainly limited by the fall time of the driving electrical signal, and is estimated to be about 5 ns.

1. Richards, B. S. Luminescent layers for enhanced silicon solar cell performance: Down-conversion. *Sol. Energy Mater. Sol. Cells* **90**, 1189–1207 (2006).
2. Kovalev, D., Heckler, H., Polisski, G. & Koch, F. Optical Properties of Si Nanocrystals. *Phys. Status Solidi B* **215**, 871–932 (1999).
3. Hill, N. A. & Whaley, K. B. Size dependence of excitons in silicon nanocrystals. *Phys. Rev. Lett.* **75**, 1130–1133 (1995).
4. Bsiesy, A. *et al.* Photoluminescence of high porosity and of electrochemically oxidized porous silicon layers. *Surf. Sci.* **254**, 195–200 (1991).
5. Shimizu-Iwayama, T., Kurumado, N., Hole, D. E. & Townsend, P. D. Optical properties of silicon nanoclusters fabricated by ion implantation. *J. Appl. Phys.* **83**, 6018–6022 (1998).
6. Garrido Fernandez, B. *et al.* Influence of average size and interface passivation on the spectral emission of Si nanocrystals embedded in SiO_2. *J. Appl. Phys.* **91**, 798–807 (2002).
7. Hayashi, S., Nagareda, T., Kanzawa, Y. & Yamamoto, K. Photoluminescence of Si-Rich SiO_2 Films: Si Clusters as Luminescent Centers. *Jpn. J. Appl. Phys.* **32**, 3840–3845 (1993).
8. Yuan, Z. *et al.* Silicon nanocrystals as a photoluminescence down shifter for solar cells. *Sol. Energy Mater. Sol. Cells* **95**, 1224–1227 (2011).
9. Giannini, V., Fernández-Domínguez, A. I., Heck, S. C. & Maier, S. A. Plasmonic Nanoantennas: Fundamentals and Their Use in Controlling the Radiative Properties of Nanoemitters. *Chem. Rev.* **111**, 3888–3912 (2011).
10. Anger, P., Bharadwaj, P. & Novotny, L. Enhancement and Quenching of Single-Molecule Fluorescence. *Phys. Rev. Lett.* **96** (2006).
11. Kühn, S., Håkanson, U., Rogobete, L. & Sandoghdar, V. Enhancement of Single-Molecule Fluorescence Using a Gold Nanoparticle as an Optical Nanoantenna. *Phys. Rev. Lett.* **97** (2006).
12. Gérard, D. *et al.* Nanoaperture-enhanced fluorescence: Towards higher detection rates with plasmonic metals. *Phys. Rev. B* **77** (2008).
13. Viste, P. *et al.* Enhancement and Quenching Regimes in Metal- Semiconductor Hybrid Optical Nanosources. *Acs Nano* **4**, 759–764 (2010).
14. Wang, Y.-L. *et al.* Plasmon-Enhanced Light Harvesting of Chlorophylls on Near-Percolating Silver Films via One-Photon Anti-Stokes Upconversion. *Sci. Rep.* **3**, 1861; DOI:10.1038/srep01861 (2013).
15. Biteen, J. S., Pacifici, D., Lewis, N. S. & Atwater, H. A. Enhanced Radiative Emission Rate and Quantum Efficiency in Coupled Silicon Nanocrystal-Nanostructured Gold Emitters. *Nano Lett.* **5**, 1768–1773 (2005).
16. Biteen, J. S., Lewis, N. S., Atwater, H. A., Mertens, H. & Polman, A. Spectral tuning of plasmon-enhanced silicon quantum dot luminescence. *Appl. Phys. Lett.* **88**, 131109 (2006).
17. Gong, Y., Lu, J., Cheng, S.-L., Nishi, Y. & Vučković, J. Plasmonic enhancement of emission from Si-nanocrystals. *Appl. Phys. Lett.* **94**, 013106 (2009).
18. Takeda, E., Fujii, M., Nakamura, T., Mochizuki, Y. & Hayashi, S. Enhancement of photoluminescence from excitons in silicon nanocrystals via coupling to surface plasmon polaritons. *J. Appl. Phys.* **102**, 023506 (2007).
19. Takeda, E., Nakamura, T., Fujii, M., Miura, S. & Hayashi, S. Surface plasmon polariton mediated photoluminescence from excitons in silicon nanocrystals. *Appl. Phys. Lett.* **89**, 101907 (2006).
20. Mochizuki, Y., Fujii, M., Hayashi, S., Tsuruoka, T. & Akamatsu, K. Enhancement of photoluminescence from silicon nanocrystals by metal nanostructures made by nanosphere lithography. *J. Appl. Phys.* **106**, 013517 (2009).
21. Zacharias, M. *et al.* Size-controlled highly luminescent silicon nanocrystals: A SiO/SiO_2 superlattice approach. *Appl. Phys. Lett.* **80**, 661 (2002).
22. Naciri, A. E. *et al.* Optical properties of uniformly sized silicon nanocrystals within a single silicon oxide layer. *J. Nanoparticle Res.* **15**, 1–9 (2013).
23. Averboukh, B. *et al.* Luminescence studies of a Si/SiO2 superlattice. *J. Appl. Phys.* **92**, 3564–3568 (2002).
24. Ureña, E. B. *et al.* Excitation Enhancement of a Quantum Dot Coupled to a Plasmonic Antenna. *Adv. Mater.* **24**, OP314–OP320 (2012).
25. Lieb, M. A., Zavislan, J. M. & Novotny, L. Single-molecule orientations determined by direct emission pattern imaging. *J. Opt. Soc. Am. B* **21**, 1210–1215 (2004).
26. Wenger, J. *et al.* Emission and excitation contributions to enhanced single molecule fluorescence by gold nanometric apertures. *Opt. Express* **16**, 3008–3020 (2008).
27. Linnros, J., Lalic, N., Galeckas, A. & Grivickas, V. Analysis of the stretched exponential photoluminescence decay from nanometer-sized silicon crystals in SiO_2. *J. Appl. Phys.* **86**, 6128 (1999).
28. Jambois, O., Rinnert, H., Devaux, X. & Vergnat, M. Photoluminescence and electroluminescence of size-controlled silicon nanocrystallites embedded in SiO_2 thin films. *J. Appl. Phys.* **98**, 046105 (2005).
29. Lopez, M. *et al.* Elucidation of the surface passivation role on the photoluminescence emission yield of silicon nanocrystals embedded in SiO_2. *Appl. Phys. Lett.* **80**, 1637–1639 (2002).
30. Ledoux, G., Gong, J. & Huisken, F. Effect of passivation and aging on the photoluminescence of silicon nanocrystals. *Appl. Phys. Lett.* **79**, 4028–4030 (2001).

Acknowledgements

We thank Alexandre Bouché for SiNC preparation. We are also grateful to Michel Vergnat for many enlightening discussions. This work has been supported by the French National Research Agency (grants HYNNA ANR-10-BLAN-1016 and TWINS ANR-11-BS10-002). Financial support of NanoMat (www.nanomat.eu) by the "Ministère de l'enseignement supérieur et de la recherche," the "Conseil régional Champagne-Ardenne," the "Fonds Européen de Développement Régional (FEDER)," and the "Conseil général de l'Aube" is acknowledged. Support from ICEEL institute and CNRS (grant MELUSINE) is also acknowledged.

Author contributions

J.G. constructed the optical setup, performed the experiments and analyzed data. D.G., P.M. and J.P. conceived the project and designed the experiments. J.G., P.M. and A.-L.B.

fabricated the structures. R.D. constructed the time-resolved PL setup and data acquisition system. J.G. and D.G. wrote the paper. All authors discussed the results and reviewed the manuscript.

Additional information

Supplementary information accompanies this paper at http://www.nature.com/scientificreports

Competing financial interests: The authors declare no competing financial interests.

How to cite this article: Goffard, J. *et al.* Plasmonic engineering of spontaneous emission from silicon nanocrystals. *Sci. Rep.* **3**, 2672; DOI:10.1038/srep02672 (2013).